# IMPROVING RIDE COMFORT AND TRACKWEAR OF TWO-AXLE RAILWAY VEHICLES USING INERTER-BASED LATERAL SUSPENSION LAYOUTS

Timothy D. Lewis[1*], Jason Z. Jiang[1*], Simon A. Neild[1], Cencen Gong[2] and Simon D. Iwnicki[3]

[1]University of Bristol: Department of Mechanical Engineering, Queens Building
University Walk, Bristol, UK, BS8 1TR
[*]Emails: tl1485@my.bristol.ac.uk, z.jiang@bristol.ac.uk

[2] Rail and Transit Infrastructure department, SNC Lavalin,
9A Devonshire Square, London, UK, EC2M 4YN

[3] School of Computing and Engineering, University of Huddersfield,
Queensgate, Huddersfield, HD1 3DH, UK

## ABSTRACT

*This paper investigates the use of passive, inerter based lateral suspension networks in two-axle railway vehicles with the aim of concurrently improving ride comfort under straight running conditions and reducing trackwear under curving conditions. It is found that employing optimised networks which include single parallel inerters can reduce the carbody acceleration by up to 43% when the vehicle is travelling over a rough track modelled either from real or random track data. $T\gamma$ is then used to quantify the frictional energy lost at the contact patch and it is found that simultaneously incorporating single parallel inerters into the lateral suspension networks and reducing the vehicle's yaw stiffness reduces trackwear and improves ride comfort. Look-up plots of optimised suspension elements for differing values of yaw stiffness are produced, with the series inerter requiring a much higher inertance than the parallel inerter when considering the most beneficial structure.*

## 1 INTRODUCTION

The trade-off between reducing railway vehicles' lateral acceleration whilst on a straight track, and reducing the magnitude of the wheel-rail contact patch curving forces has long been problematic. When a railway vehicle travels around a curve, a lower static longitudinal suspension stiffness (yaw stiffness) results in a decrease in the energy lost due to friction at the contact patch, which is quantified in this paper by the parameter commonly used in industry, $T\gamma$. However, this leads to an increase in the lateral acceleration of the vehicle body during straight track conditions, causing a deterioration in ride comfort. Decreasing $T\gamma$ reduces wear and prolongs the service life of the track and wheels, whereas improving ride comfort creates a smoother passenger experience.

This paper assesses the relative merits of employing different passive inerter based lateral suspension networks. An inerter [1], equivalent to a capacitor using the force-current analogy, and with an inertance measured in kg, is a two-terminal mechanical element which exerts a force proportional to the relative acceleration between its terminals. Mechanical networks combining inerters and other two terminal devices can theoretically acheive any linear passive response. First proposed in 2002 in the form of a rack and pinion design [1], other designs have been proposed such as the ball and screw inerter in Formula One [2], hydraulic inerters [3], fluid inerters [4–6] and mechatronic inerters [7]. The inerter device can achieve a high inertance whilst its mass remains relatively low, due to mechanical gearing or other phenomena such as a helical tubing arrangement in fluid inerters. At present they are reasonably hard-wearing, with a low Mean Time Before Failure (MTBF), resulting in the fact that only institutions such as those associated with Formula

One can afford to replace them on a regular basis. It is anticipated however that as their popularity grows, and their benefits become more widely recognised, more studies will focus on inerter designs with enhanced durability. The use of inerters has recently expanded into road vehicles [8–10], buildings [11–13] and optical tables [14].

Active methods of controlling railway vehicles have been successfully studied in [15–17], with a wide range of control laws being established. However, phenomena such as measurement error, fault tolerances, and actuator malfunction are problematic, along with the very high amount of torque required. This paper continues the work of [18] and [19], which respectively identified benefits of using inerters to curving performance and straight running passenger comfort. The main focus of this paper concerns simultaneously improving curving performance, by reducing $T\gamma$, and improving passenger comfort by the optimisation of lateral inerter based suspension networks. Both real and random track data is used to model the straight running lateral track disturbances, passenger comfort is assessed for a range of vehicle velocities, and trade-off plots of the two conflicting optimisation criteria are constructed.

The structure of this paper is as follows: Section 2 provides an overview of the model and the transfer function method of calculation, Section 3 assesses the extent to which passenger comfort can be improved by employing inerter based lateral suspension layouts, in Section 4, $T\gamma$ is established as a measure of trackwear and a trade-off plot of minimised RMS carbody acceleration vs $T\gamma$ is shown for two inerter based suspension layouts, along with various parameter look-up tables. Finally, overall conclusions are drawn in Section 5.

## 2 MODEL LAYOUT

A relatively simple, freight type railway vehicle model has been chosen for the analysis in this paper (see Figure 1(a)). It comprises the vehicle body (carbody) and two solid axle wheelsets connected to the carbody with suspension configurations $Y(s)$ and $Z(s)$ in the lateral and longitudinal direction respectively. Figure 1(b) shows the five lateral networks, three of which include inerters, and the single longitudinal network used in the analysis. The six governing equations of motion for the model are shown in Equations 1 - 6, with parameters defined in Table 1, and $s$ denoting the Laplace variable. The states are defined in Figure 1(a) and shown in Equation 7, and in Equations 1 - 6, $\hat{y}_{w1}$ represents the Laplace Transform of $y_{w1}(t)$, $\hat{\theta}_{w1}$ of $\theta_{w1}(t)$ and so on. $Y(s)$ and $Z(s)$ in Equations 1 - 6 denote the mechanical admittances of the networks from Figure 1(b) being analysed.

The 6 Degree of Freedom (DOF) model is entirely in the horizontal plane, with no vertical, roll or pitch modes included. The longitudinal direction is defined as pointing in the direction of travel and the lateral direction perpendicular to this.

The external forces acting on the model come about from the radius of curvature of the track, the cant angle of the track, and the straight running track lateral displacement. The internal forces arise from the suspension configurations $Y(s)$ and $Z(s)$, along with the creep forces at the wheel-rail contact points and gravitational stiffness. Nonlinear friction saturation is not included and it is assumed that the track is infinitely stiff. The contact angle parameter, $\varepsilon$, which introduces the gravitational stiffness and spin creepage terms is evaluated in Equation 8, taken from [20].

$$m_w s^2 \hat{y}_{w1} = 2sY(s)(\hat{y}_v - \hat{y}_{w1}) - \frac{2f_{22}}{V} s\hat{y}_{w1} + 2f_{22}\hat{\theta}_{w1} + 2sY(s)l_{wx}\hat{\theta}_v + \frac{2\varepsilon(N - f_{23})}{l_{wy}r_0}\hat{y}_{w1} + m_w\left(\frac{V^2}{R_1} - g\theta_{c1}\right) \quad (1)$$

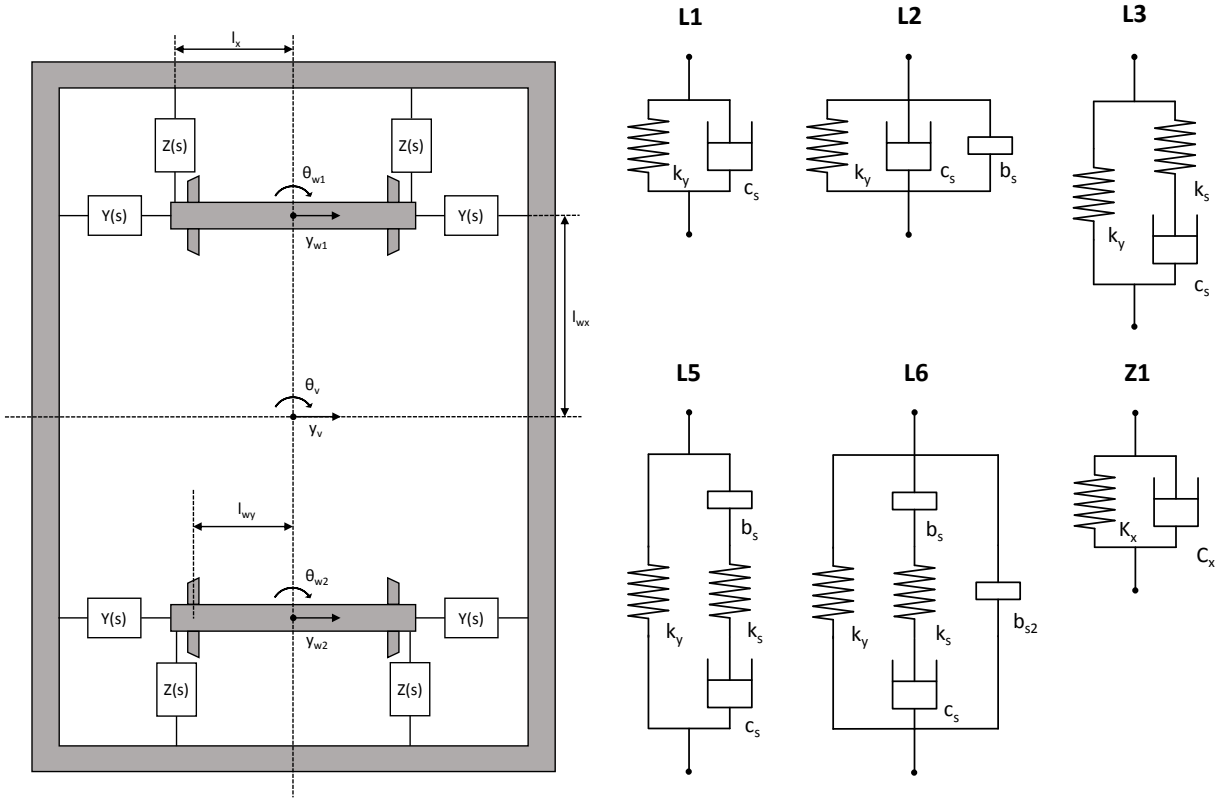


Figure 1: (a) The two-axle, zero-bogie railway vehicle model showing the two wheelsets, the carbody, and the four lateral and longitudinal suspension positions. (b) The five lateral suspension networks, $Y(s)$, along with the single longitudinal suspension network, $Z(s)$.

$$I_w s^2 \hat{\theta}_{w1} = \frac{2f_{11} l_{wy}^2}{V} s\hat{\theta}_{w1} - \frac{2f_{11}\lambda l_{wy}}{r_0}\hat{y}_{w1} + 2sZ(s)l_x^2(\hat{\theta}_v - \hat{\theta}_{w1}) - \frac{2f_{11}\lambda l_{wy}}{r_0}\hat{y}_{t1} + \frac{2f_{11}L_{wy}^2 + K_x L_{wx}}{R_1} \quad (2)$$

$$m_w s^2 \hat{y}_{w2} = 2sY(s)(\hat{y}_v - \hat{y}_{w2}) - \frac{2f_{22}}{V} s\hat{y}_{w2} + 2f_{22}\hat{\theta}_{w2} + 2Y(s)l_{wx}\hat{\theta}_v + \frac{2\varepsilon(N - f_{23})}{l_{wy} r_0}\hat{y}_{w2} + m_w\left(\frac{V^2}{R_2} - g\theta_{c2}\right) \quad (3)$$

$$I_w s^2 \hat{\theta}_{w2} = \frac{2f_{11} l_{wy}^2}{V} s\hat{\theta}_{w2} - \frac{2f_{11}\lambda l_{wy}}{r_0}\hat{y}_{w2} + 2sZ(s)l_x^2(\hat{\theta}_v - \hat{\theta}_{w2}) - \frac{2f_{11}\lambda l_{wy}}{r_0}\hat{y}_{t2} + \frac{2f_{11}L_{wy}^2 - K_x L_{wx}}{R_2} \quad (4)$$

$$m_v s^2 \hat{y}_v = 2sY(s)(\hat{y}_{w1} - \hat{y}_v) + 2sY(s)(\hat{y}_{w1} - \hat{y}_v) + \frac{m_v V}{2}\left(\frac{1}{R_1} + \frac{1}{R_2}\right) - \frac{m_v g}{2}(\theta_{c1} + \theta_{c2}) \quad (5)$$

$$I_v s^2 \hat{\theta}_v = 2sY(s)l_{wx}(\hat{y}_{w1} - \hat{y}_v) + 2sY(s)l_{wx}(\hat{y}_v - \hat{y}_{w2}) + 2sZ(s)l_x^2(\hat{\theta}_{w1} - \hat{\theta}_v) + 2sZ(s)l_x^2(\hat{\theta}_{w2} - \hat{\theta}_v) - 4sY(s)l_{wx}^2\hat{\theta}_v \quad (6)$$

$$x = [y_{w1}, \theta_{w1}, y_{w2}, \theta_{w2}, y_v, \theta_v]^T \quad (7) \qquad \varepsilon = A_c(\lambda - \lambda_0) \quad (8)$$

| Symbol | Parameter | Unit | Value |
|---|---|---|---|
| $V$ | Forward vehicle velocity | $ms^{-1}$ | 31 |
| $m_w$ | Wheelset mass | $kg$ | $1.25\times10^3$ |
| $I_w$ | Wheelset yaw inertia | $kgm^2$ | 700 |
| $m_v$ | Carbody mass | $kg$ | $3\times10^4$ |
| $I_v$ | Carbody yaw inertia | $kgm^2$ | $5.58\times10^5$ |
| $l_x$ | Semi-lateral suspension spacing | $m$ | 1 |
| $l_{wx}$ | Half the wheelset spacing | $m$ | 4.5 |
| $l_{wy}$ | Half the vehicle gauge | $m$ | 0.7 |
| $\lambda$ | Wheel conicity | – | 0.2 |
| $\lambda_0$ | Base cone profile | – | 0.05 |
| $r_0$ | Nominal wheel radius | $m$ | 0.45 |
| $y_{t1}$ | Lateral track displacement at front | – | – |
| $y_{t2}$ | Lateral track displacement at rear | – | – |
| $R_1$ | Radius of curved track at front | $m$ | $1\times10^3$ |
| $R_2$ | Radius of curved track at rear | $m$ | $1\times10^3$ |
| $\theta_{c1}$ | Cant angle of curved track at front | $rad$ | $\pi/30$ |
| $\theta_{c2}$ | Cant angle of curved track at rear | $rad$ | $\pi/30$ |
| $g$ | Gravitational acceleration | $ms^{-2}$ | 9.81 |
| $k_y$ | Lateral stiffness per axle box | $Nm^{-1}$ | $2.555\times10^5$ |
| $K_x$ | Primary lateral stiffness | $Nm^{-1}$ | $1\times10^6$ |
| $C_x$ | Primary lateral damping | $Nsm^{-1}$ | $4\times10^3$ |
| $A_l$ | Lateral track roughness factor | $m$ | $1.886\times10^{-9}$ |
| $v$ | Poisson's ratio of steel | – | 0.3 |
| $E$ | Young's Modulus of steel | $Pa$ | $2\times10^{11}$ |
| $N$ | Contact patch normal force | $N$ | $7.971\times10^4$ |
| $A_c$ | Contact angle constant | – | 50.7 |
| $C_{11}$ | Longitudinal Kalker coefficient | – | 1.65 |
| $C_{22}$ | Lateral Kalker coefficient | – | 1.43 |
| $C_{23}$ | Spin Kalker coefficient | – | 0.579 |

Table 1. Table of parameters, along with their symbols, units, and nominal values (if applicable).

A semi-state-space Laplace equation,

$$s^2x = Ax + Bu, \quad (9)$$

is formed via the manipulation of Equations 1 - 6. The system matrix, A, is a 6 by 6 matrix of transfer functions with varying powers of $s$, capturing stiffness, damping, and inertance like terms. Matrix B captures the external forcing dynamics, denotes the coefficients of the input terms, and its size depends on the number of inputs. Passenger comfort is assessed during straight running

conditions, on a flat track, with the two inputs being the front and rear lateral track displacement, resulting in a B matrix of size 6 by 2. However, when assessing curving performance, it is assumed that the track consists of no lateral displacement and the inputs are only the cant angle and radius of curvature, resulting in the B matrix being of size 6 by 4. u is the input matrix which consists of either a timeseries of lateral track displacements (either from real track data or filtered white noise, see Section 3) for the passenger comfort case, or a ramped timeseries of cant angle and radius of curvature for the curving performance case. The resulting matrix of transfer functions $H_\omega$ is given by

$$H_\omega = (s^2 I - A)^{-1} B. \tag{10}$$

This can then be employed in Simulink to calculate resulting displacements, velocities and accelerations of all six states. $I$ denotes the 6 by 6 identity matrix.

## 3 PASSENGER COMFORT IMPROVEMENT

When assessing the passenger comfort of the vehicle, the Root Mean Squared (RMS) value of lateral acceleration of the carbody, ${J_{5y}}^2$, is used as the cost function. The B matrix, which is formed by extracting the lateral track displacement ($\hat{y}_{t1}$ and $\hat{y}_{t2}$) coefficients from Equations 1 - 6, is given by

$$B = \begin{bmatrix} 0 & 0 \\ \dfrac{-2f_{11}\lambda l_{wy}}{r_0 m_w} & 0 \\ 0 & 0 \\ 0 & \dfrac{-2f_{11}\lambda l_{wy}}{r_0 m_w} \\ 0 & 0 \\ 0 & 0 \end{bmatrix}. \tag{11}$$

The calculation of the RMS value of the cardody's lateral acceleration, $A(t)$, which forms the performance criteria uses

$${J_{5y}}^2 = \int_0^\infty |A(t)|^2 \, dt. \tag{12}$$

Two different types of track input used are:

- *Real track data*: This comes in the form of lateral track displacement for a 5km stretch of track. Data for a track with a rated speed of 110km/hour is defined as Track110, and with the knowledge of the vehicle's velocity, and hence also the time delay between the front and rear wheelsets, a timeseries of this track's lateral displacement can be obtained and used as inputs $\hat{y}_{t1}$ and $\hat{y}_{t2}$.
- *Random track input*: In this case, the magnitude of the lateral track displacement is modelled using filtered white noise, a method developed previously in [21] and employed in [19]. The input to the filter $H_1(s)$ is the output of the single sided power spectrum $S_y(f_s)$ ($f_s$ is a spatial frequency in cycles/m), which in turn is dependent on the vehicle's velocity and the track roughness factor $A_l$ using

$$H_1(s) = \frac{21.69s^2 + 105.6s + 14.42}{s^3 + 30.64s^2 + 24.07s}, \tag{13}$$

$$S_y(f_s) = \frac{A_l}{f_s^2}, \tag{14}$$

$$S_{\dot{y}} = 4\pi^2 A_l V^2. \tag{15}$$

Parseval's Theorem, which states that the sum of the square of a function is equal to the sum of the square of it's Fourier transform, is used to enable Equation 12 to be written in the Frequency domain as

$$\int_0^\infty |A(t)|^2 \, dt = \frac{1}{2\pi} \int_0^\infty |A(jw)|^2 \, dw \tag{16}$$

Using

$${J_{5y}}^2 = \frac{1}{2\pi} \int_0^\infty \left| S_{\dot{y}} H_1(jw) G(jw)(1 - e^{-j\omega T_d}) \right|^2 dw, \tag{17}$$

$$J_{5y} = \sqrt{\frac{\Delta\omega S_{\dot{y}}}{2\pi} \sum_0^{30\pi} |H_1(jw)G(jw)(1 - e^{-j\omega T_d})|^2 \, dw}, \tag{18}$$

the resulting $J_{5y}$ is calculated, in which $G(jw)$ is the transfer function with an input of the lateral track displacement at the front wheelset, and an output of the lateral carbody acceleration.

Optimisations of parameters within each $Y(s)$ network can now be performed with the aim of minimising $J_{5y}$. A Simulink model with the Track110 timeseries as the input is used to calculate the $J_{5y}$ for the real track case, whereas only MATLAB is used to perform the summation required in Equation 18. The static lateral stiffness, $k_y$ is assumed to be constant at $2.555{\times}10^5$Nm$^{-1}$ and each of the other $Y(s)$ network parameters are optimised over, within reasonable limits. The results of the optimisations are shown in Tables 2 and 3, and summarised in Figure 2(a).

| Layout | $J_{5y}$ ms$^{-2}$ | Impr (%) | Parameter values (Nm$^{-1}$, Nsm$^{-1}$, kg) |
|---|---|---|---|
| L1 | 0.1335 | - | $c_s = 1.51{\times}10^4$ |
| L2 | 0.1201 | 10.0 | $c_s = 1.37{\times}10^4$, $b_s = 5.03{\times}10^2$ |
| L3 | 0.1335 | 0.0 | $k_s = \infty$, $c_s = 1.51{\times}10^4$ |
| L5 | 0.1302 | 2.5 | $k_s = \infty$, $c_s = 1.54{\times}10^4$, $b_s = 8.93{\times}10^3$ |
| L6 | 0.0753 | 43.6 | $k_s = 3.40{\times}10^5$, $c_s = 6.02{\times}10^4$, $b_s = 7.70{\times}10^3$, $b_{s2} = 1.16{\times}10^3$ |

Table 2. Optimisation results for reduced RMS carbody acceleration using Track110.

It is clear from Tables 2 and 3, and Figure 2(a) that layouts L2 and L6 provide an increasingly improved $J_{5y}$ reduction, which is most likely due to the presence of a single, parallel inerter in each. Studying Figure 2(a) we can claim that the random track theoretically describes a track with a velocity rating below 110km/hour. The optimisation process using the random track input is faster than using Track110 however due to the substantial difference in the Power Spectral Density (PSD) curves for both track types (Track110 peaks at a higher frequency than the random track), Track110 will be used for the rest of the analysis in this paper.

| Layout | $J_{5y}$ ms$^{-2}$ | Impr (%) | Parameter values (Nm$^{-1}$, Nsm$^{-1}$, kg) |
|---|---|---|---|
| L1 | 0.1011 | - | $c_s = 1.44\times10^4$ |
| L2 | 0.0912 | 9.8 | $c_s = 1.32\times10^4$, $b_s = 4.80\times10^2$ |
| L3 | 0.1008 | 0.3 | $k_s = \infty$, $c_s = 1.43\times10^4$ |
| L5 | 0.0987 | 2.4 | $k_s = \infty$, $c_s = 1.48\times10^4$, $b_s = 9.84\times10^3$ |
| L6 | 0.0571 | 43.5 | $k_s = 2.92\times10^5$, $c_s = 5.03\times10^4$, $b_s = 6.50\times10^3$, $b_{s2} = 1.02\times10^3$ |

Table 3. Optimisation results for reduced RMS carbody acceleration using the Random track.

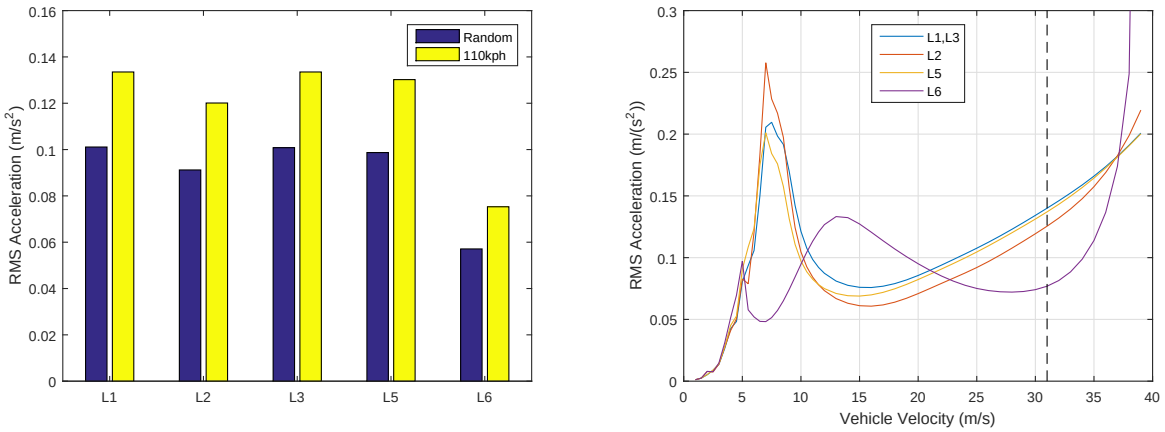


(a) (b)

Figure 2: (a) Bar chart displaying the minimised carbody RMS acceleration values for both the random track and Track110. (b) RMS carbody acceleration vs vehicle velocity for Track110, with the speed at optimisation, 31ms$^{-1}$, highlighted. Note that L1 and L3 produce the same curve as the series spring stiffness in L3 consistently optimises to infinity.

Figure 2(b) shows how the RMS carbody acceleration changes with an increase in vehicle velocity for the five lateral suspension networks, using Track110. For each configuration all parameter values remain constant as the velocity changes, as it would be unrealistic for a vehicle to have differing, and re-optimised suspension values for each intermediate speed. The vertical dashed line indicates a velocity of 31ms$^{-1}$ and the RMS accelerations here correspond with the values shown in Figure 2(a). It can be seen that in general L6 is the most optimum configuration. Only the in intermediate region between 12ms$^{-1}$ and 22ms$^{-1}$ is L6 not just sub-optimum, but the most detrimental to the RMS acceleration, however in reality the vehicle will spend little time at this speed, and furthermore the higher accelerations seen in all other configurations between 5ms$^{-1}$ and 10ms$^{-1}$ do not exist when L6 is used. Extrapolating from the highest velocities in this plot, it can be assumed that the presence of a single parallel inerter causes the RMS acceleration to increase rapidly, hence if the vehicle's speed increases much above 37ms$^{-1}$ the passenger comfort will reduce extremely fast, however this would mean that the vehicle's rated speed and hence the optimisation speed would increase also.

## 4 CURVING PERFORMANCE ASSESSMENT

Whilst passenger comfort has been quantified by the extent of the carbody's lateral acceleration, curving performance is assessed by quantifying the energy lost at the contact patch, $T_\gamma$. This parameter is widely used in industry and is representative of the detrimental effects on the wheel that curving produces. The inputs to the system now are cant angle and radius of curvature, and the B matrix is of size 6 by 4:

$$B = \begin{bmatrix} V^2 & -g & 0 & 0 \\ \frac{2(f_{11}l_{wy}^2 + K_x L_{wx} l_x^2)}{Iw} & 0 & 0 & 0 \\ 0 & 0 & V^2 & -g \\ 0 & 0 & \frac{2(f_{11}l_{wy}^2 - K_x L_{wx} l_x^2)}{Iw} & 0 \\ V^2/2 & -g/2 & V^2/2 & -g/2 \\ \frac{-2K_x L_{wx} l_x^2}{Iv} & 0 & \frac{2K_x L_{wx} l_x^2}{Iv} & 0 \end{bmatrix} \tag{19}$$

The following description of the calculation of $T_\gamma$ focuses only on the left wheel on the front wheelset, however the theory can be applied to every wheel. An average value of these four $T_\gamma$ values is used when presenting data in the latter part of Section 4. The longitudinal and lateral creepages, $v_{x1l}$ and $v_{y1l}$,

$$v_{x1l} = \frac{l_{wy}\dot{\theta_{w1}}}{V} + \frac{\lambda y_{w1}}{r_0} - \frac{l_{wy}}{R_1}, \tag{20}$$

$$v_{y1l} = \frac{\dot{y_{w1}}}{V} - \theta_{w1}, \tag{21}$$

denote the extent of the relative velocity between the wheel and rail, and the spin creepage, $v_{z1l}$,

$$v_{z1l} = \frac{\varepsilon}{r_0 l_{wy}} y_{w1}, \tag{22}$$

arising from the thickness of the contact patch, includes the contact angle parameter, $\varepsilon$, from [20]. The contact patch dimension product, $ab$,

$$ab = \left[\frac{1.5(1-v^2)Nr_0}{E}\right]^{2/3}, \tag{23}$$

is dependent on the average normal force of the vehicle per wheel, $N$, Poisson's Ratio of steel, $v$, and the nominal wheel radius, $r_0$. To convert the creepages into creep forces, the creep force coefficients $f_{11}$, $f_{22}$ and $f_{23}$,

$$f_{11} = Ec_{11}ab, \tag{24}$$

$$f_{22} = Ec_{22}ab, \tag{25}$$

$$f_{23} = Ec_{23}ab, \tag{26}$$

which depend on the Kalker coefficients $c_{11}$, $c_{22}$ and $c_{23}$ [22] are determined. The longitudinal and lateral creep forces, respectively $F_{x1l}$ and $F_{y1l}$,

$$F_{x1l} = f_{11}v_{x1l}, \tag{27}$$

$$F_{y1l} = f_{22}v_{y1l} + f_{23}v_{z1l}, \tag{28}$$

can then be calculated leading on to $T_\gamma$ [23],

$$T_{\gamma 1l} = F_{x1l} v_{x1l} + F_{y1l} v_{y1l}. \tag{29}$$

It is worth noting that $T_\gamma$ is often expressed in N, and depends on the square of both the lateral and longitudinal creepages. This analysis assumes dry, clean conditions with a coefficient of friction value of $\mu = 0.6$, and a linear creep vs creep force relationship.

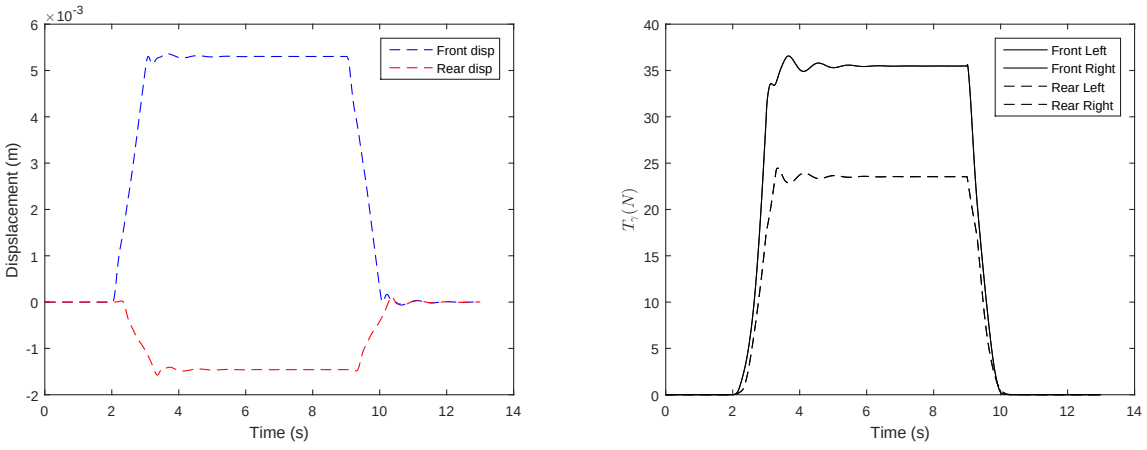


(a) (b)

Figure 3: (a) Front and rear wheelset displacement vs time, for $K_x = 3{\times}10^6 Nm^{-1}$. (b) $T\gamma$ vs time, for $K_x = 3{\times}10^6 Nm^{-1}$.

Figures 3(a) and 3(b) show respectively the $T\gamma$ and lateral wheelset displacement responses to the curving inputs defined at the start of Section 4, for a yaw stiffness value of $3{\times}10^6$Nm$^{-1}$. It is found that $T_\gamma$ is highly dependent on the yaw stiffness, due to increasing $K_x$ highly correlating with an increasing steady state curving displacement, hence higher longitudinal creep forces. Therefore, for the beneficial structures L2 and L6, RMS acceleration minimisation by optimisation of the lateral suspension parameters is performed for 11 values of $K_x$ (increasing from $1{\times}10^6$Nm$^{-1}$ to $6{\times}10^6$Nm$^{-1}$ in steps of $0.5{\times}10^6$Nm$^{-1}$) with the results shown in the trade-off plot of Figure 4(a).

In Figure 4(a) each dot-dashed line connects points of equal yaw stiffness (which increase with increasing $T\gamma$) and hence it is clear that the most beneficial of the two structures is L6 as it permits a reduced straight running RMS acceleration for a given acceptable $T\gamma$ during curving. From this plot it can be concluded that although the use of single parallel inerters in the lateral based suspension networks does not directly reduce $T\gamma$, it enables the yaw stiffness to be reduced for a given RMS acceleration during straight running, which in turn allows for a reduction in $T\gamma$, and in the case of Figure 4(a), the RMS carbody acceleration also. For example, at the point on the L2 curve where $K_x$ = $2{\times}10^6$Nm$^{-1}$, RMS acceleration = 0.102ms$^{-2}$ and $T_\gamma$ = 12.959N. If instead the L6 layout is used, and the yaw stiffness is reduced by $1{\times}10^6$Nm$^{-1}$, values of 0.075ms$^{-2}$ and 3.193N can be achieved, respectively providing improvements of 26.5% and 75.36%.

Figures 4(b), 5(a) and 5(b) display how each of the optimised parameter values of L2 and L6 vary with increasing yaw stiffness - and hence act as a look-up plots. The downside to employing the beneficial L6 network is that a high value of the series damping, $c_s$, and the series inertance, $b_s$ is required compared to L2. Manufacturing inerters with increased levels of inertance is feasible (by adding more gearing and increasing the piston-tube cross sectional area in mechanical and fluid inerters respectively), but only to a certain extent. The near-linear increase in the L6 series stiffness in Figure 4(b) is as expected due to an overall stiffening of the system following a higher yaw stiffness, and it remains very much within reasonable limits. The reason behind the more

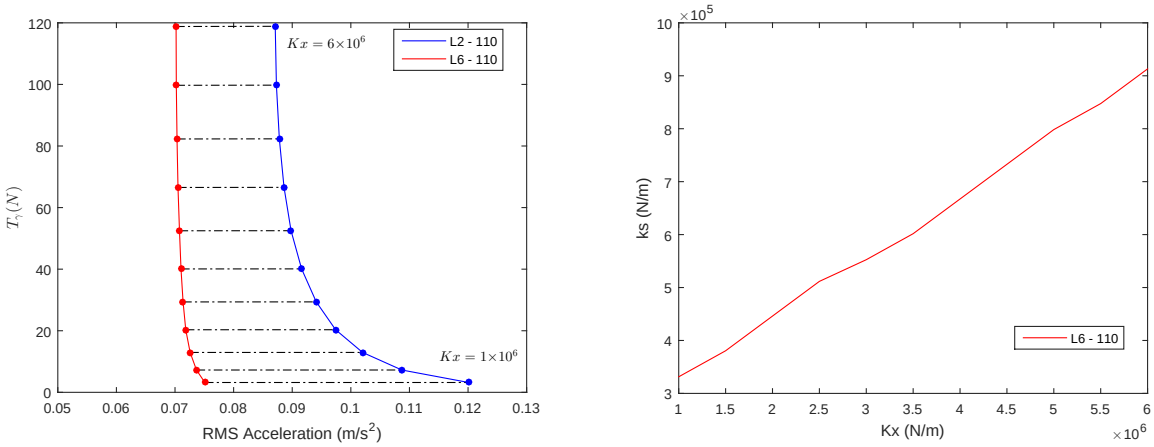


(a) (b)

Figure 4: (a) A trade-off plot showing $T\gamma$ vs optimised RMS acceleration for different values of $K_x$, and for L2 and L6 lateral suspension configurations. As the yaw stiffness increases, the RMS acceleration decreases, but $T\gamma$ increases. (b) Optimised $k_s$ values vs $K_x$ for the L6 configuration. L2 does not contain any springs other than the static stiffness $k_y$.

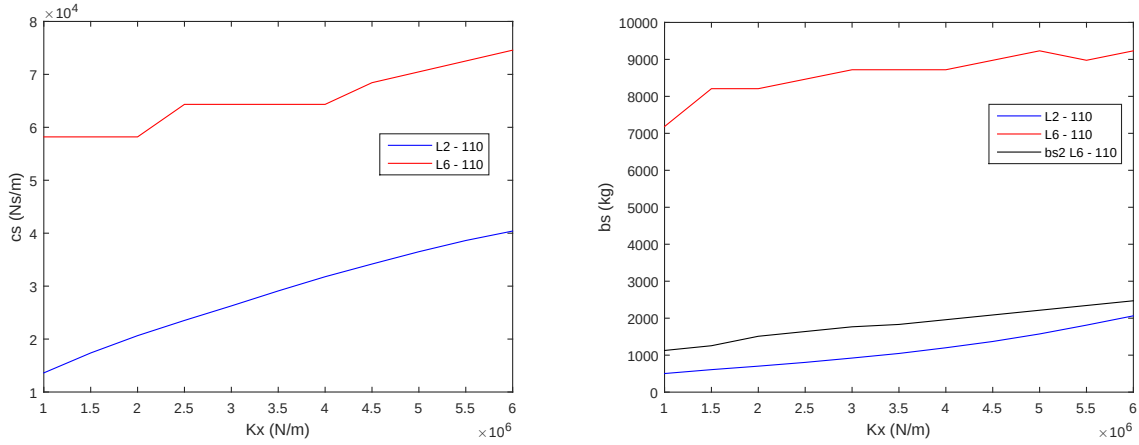


(a) (b)

Figure 5: (a) Optimised $c_s$ values vs $K_x$ for the L2 and L6 configurations. (b) Optimised $b_s$ values vs $K_x$ for the L2 and L6 configurations.

scattered increase in the L6 parameters is most likely due to the fact that the optimisation process becomes increasingly dependent on initial conditions with a higher lateral network complexity, though meaningful conclusions can still be drawn from the general trends.

## 5 CONCLUSIONS

This paper has investigated how the use of inerters in the lateral suspension of a two-axle railway vehicle reduces trackwear, quantified by the energy lost at the contact patch, $T_\gamma$, when the vehicle is in a curve, and improves passenger comfort, quantified by the RMS carbody acceleration, when the vehicle is running along a straight track. RMS acceleration reduction optimisations have been performed on five inerter based layouts and it has been found that layout L6, which includes a series and parallel inerter can achieve a RMS acceleration reduction of 43%. Investigations

using both real track data and a random lateral track disturbance produce very similar results. Curving analysis concludes that although the use of single parallel inerters in the lateral suspension networks cannot directly reduce $T\gamma$, it enables the yaw stiffness to be reduced whilst maintaining, or in most cases reducing RMS acceleration during straight running, which in turn allows for a reduction in $T\gamma$. There is much scope for the trade-off plot, displayed in this paper, to be extended into an exhaustive trade-off plot which allows the correct optimised network parameters to be chosen according to how important ride comfort or trackwear is for a particular railway vehicle and its operating conditions.

From a financial perspective, the findings are very beneficial as a reduction in the energy lost at the contact patch will result in a greater Mean Time Before Failure of wheels and rails, along with reduced maintenance costs. Another benefit to this investigation is that employing entirely passive devices in the suspension systems of railway vehicles alleviates the need for very expensive and large actuators with high torque requirements, further reducing costs.

There is much scope for further research into the use of inerters in railway vehicles. Most notably, performing optimisations of both lateral and longitudinal inerter based suspension systems could yield even higher reductions in RMS carbody acceleration, and also the modelling of a full passenger vehicle (two bogies, four axles) could strengthen the findings, along with validation using a scaled vehicle model.

## ACKNOWLEDGMENTS

The authors would like to thank the EPSRC (Grant References: EP/M507994/1 and EP/P013546/1) for funding this research.

## REFERENCES

[1] Malcolm Smith. Synthesis of mechanical networks: The inerter. *IEEE Transactions on Automatic Control*, 47(10):1648–1662, 2002.

[2] Michael Z. Q. Chen, Christos Papageorgiou, Frank Scheibe, Fu-Cheng Wang, and Malcolm C. Smith. The missing mechanical circuit element. *IEEE Circuits and Sytems Magazine*, 2009.

[3] Fu-Cheng Wang, Min-Feng Hong, and Y. C. Lin. Designing and testing a hydraulic inerter. *IMECHE Mechanical Engineering Science*, 225:66–72, 2010.

[4] S. J. Swift, M. C. Smith, A. R. Glover, C. Papageorgiou, B. Gartner, and N. E. Houghton. Design and modelling of a fluid inerter. *International Journal of Control*, 86(11):2035–2051, 2013.

[5] Rhema Andrews, Alex Duncan, Timothy Lewis, and Evelynn Yang. Design, manufacture and testing of fluid inerter devices. Technical report, University of Bristol, 2015.

[6] Xiaofu Liu, Jason Zheng Jiang, Branislav Titurus, Andrew J.L. Harrison, and Daniel McBryde. Testing and modelling of the damping effects for fluid-based inerters. *Procedia Engineering*, 199:435–440, 2017.

[7] Fu-Cheng Wang and Hsiang-An Chan. Vehicle suspensions with a mechatronic network strut. *Vehicle System Dynamics*, 49(5):811–830, 2011.

[8] Frank Scheibe and Malcolm Smith. Analytical solutions for optimal ride comfort and tyre grip for passive vehicle suspensions. *Vehicle System Dynamics*, 47(10):1229–1252, 2009.

[9] Simos Evangelou, David J. N. Limebeer, Robin S. Sharp, and Malcolm C. Smith. An h infinity loop-shaping approach to steering control for high-performance motorcycles. *Lecture Notes in Control and Information Sciences*, 329:257–275, 2006.

[10] Jason Z. Jiang, Malcolm Smith, and Neil E. Houghton. Experimental testing and modelling of a mechanical steering compensator. *International Symposium on Communications, Control and Signal Processing*, pages 249–254, 2008.

[11] I. F. Lazar, S. A. Neild, and D. J. Wagg. Using an inerter-based device for structural vibration suppression. *Earthquake Engineering  Structural Dynamics*, 43:1129–1147, 2014.

[12] Fu-Cheng Wang, Cheng-Wei Chen, Min-Kai Liao, and Min-Feng Hong. Performance analyses of building suspension control with inerters. *46th IEEE Conference on Decision and Control*, 2007.

[13] Sara Ying Zhang, Jason Zheng Jiang, and Simon Neild. Optimal configurations for a linear vibration suppression device in a multi-storey building. *Structural Control and Health Monitoring*, 24(3):e1887–n/a, 2017. e1887 STC-16-0018.R2.

[14] Yu-Chuan Chen, Sheng-Yao Wu, and Fu-Cheng Wang. Vibration control of a three-leg optical table by mechatronic inerter networks. *SICE Annual Conference 2014*, 2014.

[15] Roger Goodall and T. X. Mei. Mechatronic strategies for controlling railway wheelsets with independently rotating wheels. In *2001 IEEWASME International Conference on Advanced Intelligent Mechatronics Proceedings 6-12 July 2001 Como, Italy*, pages 225–230, 2001.

[16] T. X. Mei and R. M. Goodall. Practical strategies for controlling railway wheelsets independently rotating wheels. *Journal of Dynamic Systems, Measurement, and Control*, 125:354–360, 203.

[17] T. X. Mei and Roger M. Goodall. Robust control for independently rotating wheelsets on a railway vehicle using practical sensors. *IEEE Transactions on Control Systems Technology*, 9(4):599–607, 2001.

[18] Jason Zheng Jiang, T X Mei, and Malcolm Smith. Curving performance for railway vehicles with advanced passive suspensions. In *23rd IAVSD*, 2013.

[19] Jason Zheng Jiang, Alejandra Z. Matamoros-Sanchez, Argyrios Zolotas, Roger M. Goodall, and Malcom C. Smith. Passive suspensions for ride quality improvement of two-axle railway vehicles. *IMECHE: Journal of Rail and Rapid Transit*, 229(3):315–329, 2015.

[20] Vampire help manual. Technical report, DeltaRail Group Limited, 2016.

[21] Hong Li. *Measuring Systems for Active Steering of Railway Vehicles*. PhD thesis, Loughborough University, 2001.

[22] J. J. Kalker. The computation of three-dimensional rolling contact with dry friction. *International Journal for Numerical Methods in Engineering*, 14(9):1293–1307, 1979.

[23] Mark Burstow. VTAC calculator: Guidance note for determining t$\gamma$ values, 2012.